



Cite this: *Soft Matter*, 2016, 12, 8440

## Dynamic scaling of ferromagnetic micro-rod clusters under a weak magnetic field†

Rui Cheng,<sup>a</sup> Lu Zhu,<sup>a</sup> Weijie Huang,<sup>b</sup> Leidong Mao\*<sup>a</sup> and Yiping Zhao\*<sup>b</sup>

A controlled configurational change of micro-clusters in suspensions is essential for many smart material applications. In this paper, the dynamic process of ferromagnetic microrod clusters (FMRCs) under an external magnetic field was studied as a function of the cluster size  $N$  and the applied field  $B$ . The FMRCs rearranged from a side-by-side raft-like structure to an end-to-end chain-like structure, originating from coupled motions through the field-driven alignment of both ferromagnetic microrods and FMRCs. A theoretical model based on an extension of a zig-zag chain was developed, and both the cluster length and orientation could be characterized by a retardation time constant  $\tau$ , with a relationship  $\tau \sim N^2/B$ , which agrees well with the experimental results,  $\tau \sim N^{2.2 \pm 0.2}/B^{0.8 \pm 0.1}$ . Such a model can be used to predict other cluster dynamics or the magneto-elastic behavior of other soft matters consisting of FMRCs.

Received 27th June 2016,  
Accepted 7th September 2016

DOI: 10.1039/c6sm01485b

[www.rsc.org/softmatter](http://www.rsc.org/softmatter)

## Introduction

The dynamic response of magnetic micro-/nano-particles suspended in fluids under an external magnetic field has attracted decades of attention, because of their potential applications in biosensors,<sup>1–3</sup> microfluidic actuators,<sup>4–7</sup> tunable optical and thermal filters,<sup>8–12</sup> micro-fiber fabrication,<sup>13–15</sup> and programmable smart materials.<sup>16–18</sup> Most of these applications are related to the anisotropic growth of one-dimensional clusters by magnetic particles under an external magnetic field  $B$ , which has been studied both experimentally and theoretically.<sup>19–30</sup> For superparamagnetic particles, they are treated to be nonmagnetic in the absence of a  $B$ -field and are uniformly suspended in the liquid due to Brownian motion; when a  $B$ -field is applied, the particles are magnetized and their magnetic energy overcomes the thermal energy, leading to the aggregation of the particles along the  $B$ -field direction. The average chain length  $L(t)$  is found to follow a power law with respect to time  $t$ , e.g.,  $L(t) \propto t^Z$ , where  $Z$  is the dynamic exponent.<sup>20–22,24</sup> When the  $B$ -field is removed, the magnetic interaction among the aggregation of particles vanishes and individual particles are re-suspended in the liquid. However, for ferromagnetic particles (FMPs), even

without an external  $B$ -field, they naturally aggregate to form worm-like clusters due to their remnant magnetization and interactions.<sup>19,31,32</sup> When a  $B$ -field is applied, the original clusters will experience a configuration change, *i.e.*, there is a tendency for the clusters to uncurl and align in the  $B$ -field direction, due to the magnetic interaction between the particles and the external  $B$ -field.<sup>19,32</sup> Meanwhile, clusters will merge to form longer clusters, which also makes  $L(t)$  increase as a power law with respect to  $t$ .<sup>33</sup> On the other hand, more complex structures in two dimensions and three dimensions can be formed by spherical particles with decentered magnetism, such as Janus magnetic particles<sup>34</sup> and capped magnetic particles.<sup>35</sup> Specifically, the orientation of the decentered magnetism can be either in the radial direction or in the tangential direction of the spherical particles, whose structural transition from the ground state to finite thermal fluctuation has been well studied by theoretical and numerical approaches.<sup>36,37</sup>

In addition, the geometric shape of the fundamental magnetic components plays a very important role in their dynamic response to a magnetic field, possibly leading to unique mechanical properties of the bulk material manipulated in external magnetic fields.<sup>38,39</sup> In most published works, the magnetic components in a micro cluster are spherical particles with isotropic volume exclusion. As a result, there is no orientation effect of individual particles during particle clustering under an external  $B$ -field, though the formed clusters still experience a configuration change. However, when the FMPs become anisotropic, such as a rod shape, the clustering of ferromagnetic rods (FMRS) will become much more complicated compared to that of spherical particles due to their anisotropic magnetic interaction resulting from uniaxial magnetic isotropy<sup>40,41</sup> and

<sup>a</sup> College of Engineering, University of Georgia, Athens, Georgia 30602, USA.

E-mail: mao@uga.edu; Fax: +1-706-542-3806; Tel: +1-706-542-1871

<sup>b</sup> Department of Physics and Astronomy, University of Georgia, Athens, Georgia 30602, USA. E-mail: zhaoy@physast.uga.edu; Fax: +1-706-542-2492;

Tel: +1-706-542-7792

† Electronic supplementary information (ESI) available: Details of the FMR synthesis, XRD and statistic dimensions of the FMRs, more representative plots of the FMRCs' dynamics, and the mathematical derivation of FMRC governing equations. See DOI: 10.1039/c6sm01485b

anisotropic volume exclusion. Though extensive efforts have focused on their unique properties and applications,<sup>28,42–44</sup> the clustering of FMRs is not well understood to the best of our knowledge. Aoshima and Satoh have conducted a two-dimensional (2D) Monte Carlo simulation on the clustering of FMRs without an external  $B$ -field.<sup>45</sup> They found that the FMR aggregations consist of a few fundamental structures, such as anti-parallel particle pairs, raft-like clusters, and triangle-loop-like clusters. In particular, the raft-like cluster is more stable than other structures when the aspect ratio of FMRs is larger than 2, which has been experimentally obtained by the dispersion of Nickel nanorods in poly(2-vinylpyridine) (PVP) solution.<sup>46,47</sup> They also investigated the influence of an external  $B$ -field on the rod clustering *via* a 2D Monte Carlo simulation.<sup>32</sup> It was found that adjacent FMRs align end-to-end along the  $B$ -field direction, forming two types of joints, a step-like structure in high concentration suspension and a chain-like structure in low concentration suspension. According to the simulation results, an appreciable extension of the individual rod clusters is expected due to the anisotropic volume exclusion between rods when an external  $B$ -field is applied. However, the dynamic extension of ferromagnetic rod clusters (FMRCs) has not been investigated either experimentally or theoretically under the external  $B$ -field and the mechanism is unknown. In this paper, we conducted a systematic study on the dynamic behavior of individual FMRCs under an external  $B$ -field. For the same cluster, the dynamic changes in both the cluster length and the orientation follow the same retardation time, and the retardation time obeys a scaling law of the maximum cluster size and the applied  $B$ -field. Based on a zig-zag chain structure, a theoretical model is proposed which can predict the experimental dynamics very well.

## Experimental methods

The precursors of ferromagnetic micro-rods were synthesized by a solvothermal method,<sup>48</sup> then annealed in air to remove the organic compounds, and in ethanol/ $N_2$  to reduce to  $Fe_3O_4$ .  $Fe(NO_3)_3 \cdot 9H_2O$  (0.7575 g) and glucose (0.5 g) were thoroughly dissolved into ethylene glycol (75 ml). Then the mixture was transferred into a 100 ml Teflon-lined stainless steel autoclave and maintained at a temperature of 220 °C for 12 h. The product was collected by centrifugation, and washed twice with absolute ethanol then dried in an oven at 65 °C overnight. Secondly, the microrod-shaped precursors were annealed at 600 °C for 2 h in air to obtain  $\alpha$ - $Fe_2O_3$  microrods. Finally, the  $Fe_3O_4$  microrods were prepared by annealing the  $\alpha$ - $Fe_2O_3$  rods at 350 °C for 1 h in ethanol-carried  $N_2$  flow. The crystal structures of as synthesized FMRs were characterized by an X-ray diffractometer (XRD; PANalytical X'Pert PRO MRD) equipped with a Cu K $\alpha$  source ( $\lambda = 1.5405980 \text{ \AA}$ ) at 45 kV and 40 Ma (see the ESI,† S1). The scanning electron microscope (SEM) image in Fig. 1a reveals that each rod is a porous cylinder with hemispherical ends. The length of the rods  $l = 1.0 \pm 0.3 \text{ \mu m}$ , the diameter of the rods  $d = 0.35 \pm 0.09 \text{ \mu m}$ , and the

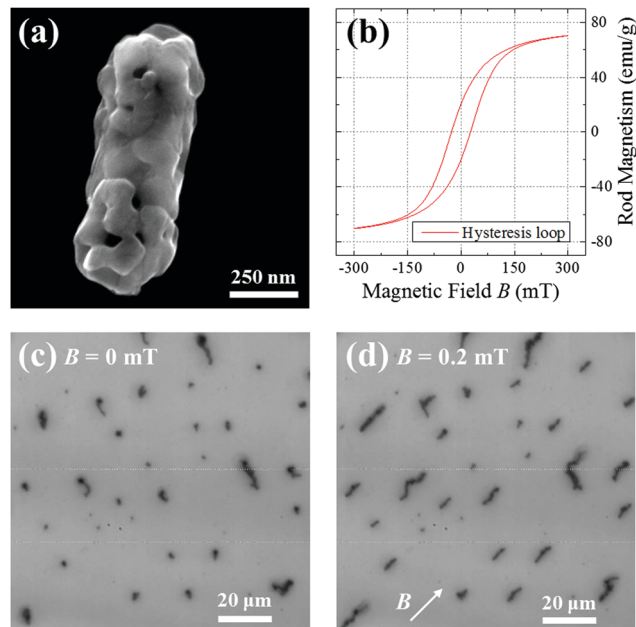


Fig. 1 (a) A representative SEM image of a single  $Fe_3O_4$  microrod. (b) The magnetic hysteresis loop of  $Fe_3O_4$  microrods. An optical microscope image of rod clusters at (c)  $B = 0 \text{ mT}$  and (d)  $B = 0.2 \text{ mT}$ . The  $B$ -field direction is indicated by a white arrow.

aspect ratio of the rods  $\gamma = l/d = 2.9 \pm 0.4$  (see the ESI,† Fig. S1). According to Butler and Banerjee's theory, the size of a single-domain particle with an aspect ratio of  $\gamma = 3$  is up to  $0.8 \text{ \mu m}$ .<sup>49</sup> It implies that some of the FMRs in our experiments may have multiple-domains with a field dependent magnetization process. However, the dynamic response of the domain walls (rotation or reorientation) to an external magnetic field is normally less than 100 ns.<sup>50–52</sup> Comparing with the time scale of the cluster motion ( $\sim 100 \text{ ms}$ ), we can safely neglect the influence of the rod magnetization process on the cluster motion and consider the rod as a single-domain magnetic particle in our model. Measurements using a vibrating sample magnetometer (VSM) (Fig. 1b) demonstrated that the residual magnetization of each rod was  $m = 20 \text{ emu g}^{-1}$  (or  $10^5 \text{ A m}^{-1}$ ) and the saturated magnetization was  $70 \text{ emu g}^{-1}$  (or  $3.5 \times 10^5 \text{ A m}^{-1}$ ). The hysteresis ratio of the saturated magnetization to the residual magnetization is around 0.3, which is lower than the theoretical value of 0.5 predicted by the Stoner–Wohlfarth model. This could be caused by the existence of small particles ( $< 100 \text{ nm}$ ) that were broken down from the rods during the annealing process in the test sample (see the ESI,† Fig. S2).<sup>53</sup>

The rods were suspended in deionized water to achieve a mass concentration of  $0.1 \text{ mg ml}^{-1}$ , corresponding to a volume fraction  $\phi \approx 2 \times 10^{-5}$ . A  $10 \text{ \mu l}$  droplet of rod suspension was dispensed in a well on a clean silicon substrate and covered by a glass slide. The well was made of a  $100 \text{ \mu m}$  thick ring-shaped plastic spacer and had a  $12.7 \text{ mm}$  inner diameter. Through an optical microscope (Mitituyua FS110), most of the rod clusters were suspended uniformly in the suspension like black scattered dots when  $B = 0 \text{ mT}$  (Fig. 1c). When a  $B$ -field ( $B = 0.2 \text{ mT}$ ) was applied, the clusters were quickly transformed from circle

dots into linear chains lying along the  $B$ -field direction (Fig. 1d). Such a dynamic process was recorded at 200 fps using a CCD camera (SLAM Solutions, Phantom v9.1). From the video (see the ESI,† Movie), the clusters maintained separation from each other and no cluster–cluster aggregation was observed.

## Results and discussion

Fig. 2a shows the snapshots of an extension process of a FMRC at every 10 ms under  $B = 1$  mT. The first frame shows the initial appearance of the FMRC, which was a circular shape ( $t = 0$  ms); when  $B = 1$  mT was applied (in the direction of the white arrow), the cluster was first transformed into a crescent shape ( $t = 10$  and 20 ms), then the crescent was opened to form a short arc ( $t = 30, 40,$  and 50 ms), and eventually the arc was extended to a straight chain ( $t = 60, 70, 80,$  and 90 ms). During this configurational change, the orientation of the cluster kept approaching the  $B$ -field direction as indicated by red arrows in Fig. 2a. To quantitatively characterize the dynamics of the cluster, we defined  $\lambda$  to be the normalized length of the cluster at time  $t$ ,  $\lambda = \frac{L}{L_s}$ , where  $L$  is the instant length and  $L_s$  is the saturated (maximum) length of the cluster, and the orientation of the cluster  $\varphi$  is the included angle between the cluster (indicated as red arrows) and the  $B$ -field. Fig. 2b plots  $\lambda$  and  $\varphi$  versus time  $t$  extracted from the movie's frames (Fig. 2a) (similar plots can be extracted from the movie frames of different clusters under different  $B$ -fields, in the ESI,† S2). When  $t$  increases from 0 to 60 ms,  $\lambda$  increases sharply from its initial value around 0.3 to 0.9. When  $t > 60$  ms,  $\lambda$  gradually approaches to a constant value of 0.971. Eventually ( $t > 100$  ms),  $\lambda$  fluctuates around this constant value. On the other hand,  $\varphi$  decreases from 1.3 concavely, approaching 0, when  $t$  changes from 0 ms to 150 ms. At  $t > 150$  ms,  $\varphi$  fluctuates around  $\varphi = 0$ . Both the fluctuations of  $\lambda$  and  $\varphi$  at large  $t$  are caused by the Brownian

diffusion of the magnetic chain.<sup>54</sup> Both Fig. 2a and b reveal the dynamic transformation of the cluster to be an extension–rotation coupled motion. Such a cluster extension and reorientation are caused by the re-arrangement of the rods in the cluster during the application of the external  $B$ -field, and is indirectly confirmed by the SEM images of FMRCs with and without the presence of the  $B$ -field, shown in Fig. 2c and d, respectively. These SEM samples were prepared by air-drying the FMRC suspensions on the silicon substrates under  $B = 0$  mT and  $B = 1$  mT, respectively. When  $B = 0$  mT, Fig. 2c shows that the rods are stacked side by side to form a raft-like cluster while some rods may form multiple layers on top of the “raft”. This indicates that the rods prefer to pack closely along their long axes, and form a relatively small cluster size. Such a structural feature is consistent with the previous experimental observation and simulation.<sup>45–47</sup> When  $B = 1$  mT, the cluster in Fig. 2d is composed mostly of a single chain with adjacent rods linked end to end, which is predicted by the Monte Carlo simulation.<sup>32</sup> Only a few small rods are packed side by side at the ends of the chain, either due to the capillary effect during the drying process, or their interaction is so strong that the  $B = 1$  mT field cannot extend them.

Clearly, the dynamic behavior under an external  $B$ -field shown in Fig. 2b is due to the configurational change of FMRCs revealed by Fig. 2c and d, which can be treated as an unfolding process. Such unfolding dynamics of scaffolding structures widely exists in biomaterials from the micrometer scale to the molecular level, such as polymers<sup>55,56</sup> and proteins,<sup>57–59</sup> and has been closely connected to their viscoelasticity. Theoretically, the unfolding process of these biomaterials are described by either a freely-jointed chain model<sup>60</sup> or a worm-like chain model.<sup>61</sup> Similarly, the  $\lambda$  and  $\varphi$  curves (Fig. 2b) exhibit the typical viscoelastic features in response to the external  $B$ -field, and the SEM images shown in Fig. 2d implies that the extended cluster behaves like a freely-jointed chain based on magnetic interaction. Thus, we propose a freely-jointed chain model to describe this dynamic process. Fig. 3a illustrates the basic idea of the model with a cluster of three FMRCs. When  $B = 0$  mT, the three FMRCs form a side-by-side cluster, with the adjacent magnetic moment  $\vec{m}$  pointing to the opposite direction (left sketch in Fig. 3a, magnetic charge indicated by the + and – signs). When an external  $B$ -field is applied, both the FMRCs and the orientation of the cluster (the center-to-center direction of FMRCs as indicated by the dash-dotted lines in the middle sketch of Fig. 3a) are driven to be aligned towards the  $B$ -field direction, and the cluster becomes a zig-zag chain as shown in the right sketch of Fig. 3a. Thus, the extension and reorientation of the FMRCs is essentially caused by the spinning of each FMRC and the rotation of the entire cluster, respectively. The two rotatory motions are associated with two angles, the angle between the cluster axis and the  $B$ -field direction  $\varphi$  and the included angle between the long axis of the rod and the principle axis of the chain  $\theta$ , as indicated in Fig. 3a. During the extension, both  $\varphi$  and  $\theta$  keep decreasing while the cluster translates from a side-by-side chain to an end-to-end chain aligned in the direction of the  $B$ -field. To account for the magnetic interactions between

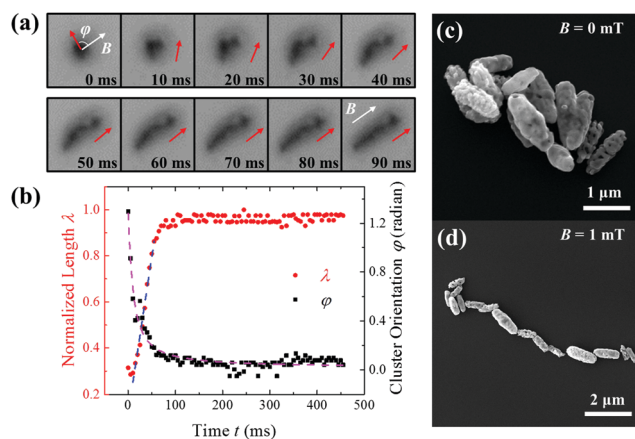
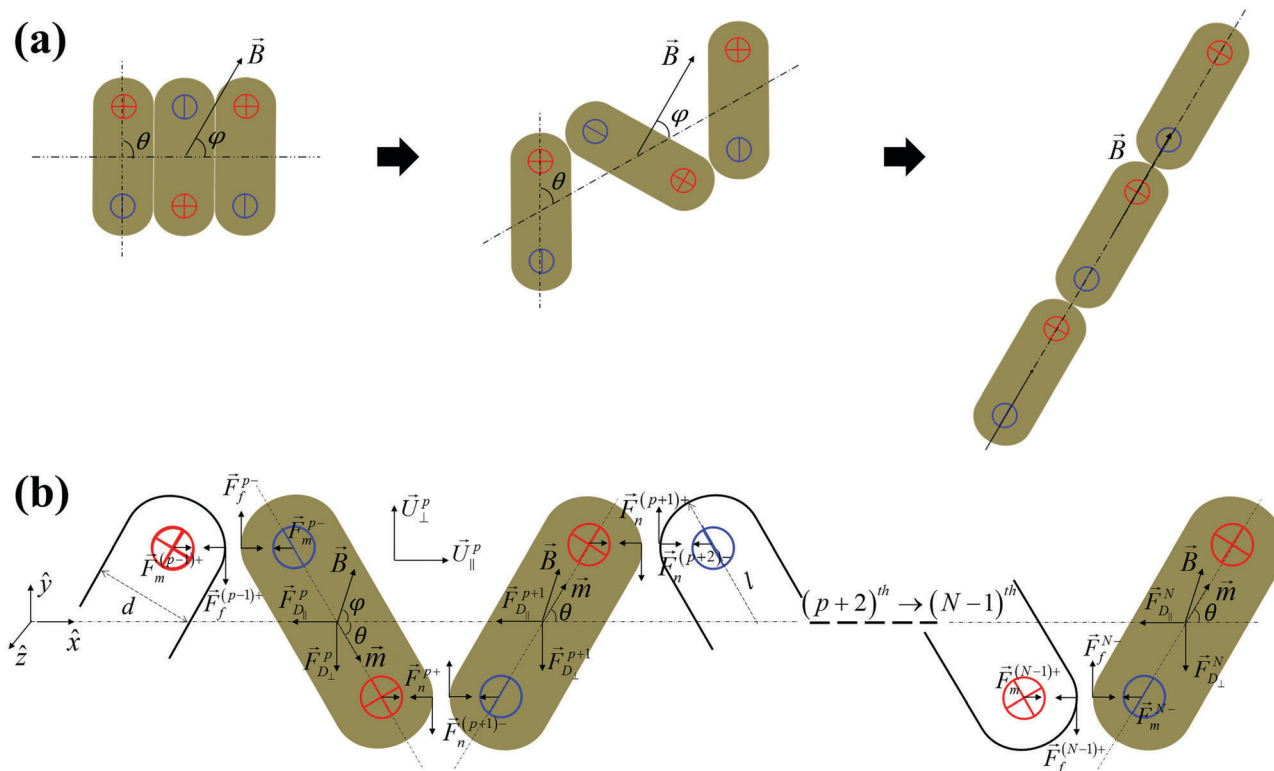


Fig. 2 (a) Representative video frames of the extension–rotation coupling motion of a FMRC with  $L_s = 9 \mu\text{m}$  at  $B = 1$  mT. (b) The plots of the normalized length  $\lambda$  (red circles) and the orientation  $\varphi$  (black squares) with respect to time  $t$ , extracted from the magnetic cluster shown in (a). The dashed curves are the fitting results. Representative SEM images of a FMRC at (c)  $B = 0$  mT, and (d)  $B = 1$  mT.



**Fig. 3** (a) The proposed dynamic process for a side-by-side chain to be extended to an end-to-end chain via a zig-zag chain model triggered by an external  $B$ -field. (b) Force and torque analysis on a pair of the  $p^{\text{th}}$  and  $(p+1)^{\text{th}}$  rods (color filled,  $1 \leq p \leq N-2$ ), and the  $N^{\text{th}}$  rod in the half chain at any time  $t$ .

FMRs and to simplify the mathematical treatment, we also make the following assumptions: (i) each rod is treated as a single domain particle with the same shape, dimension and magnetic moment  $m$  along its long axis; (ii) all the rods in one cluster are arranged in a zig-zag chain structure with the same  $\theta$  at any time  $t$ ; (iii) there is no translational motion of the entire magnetic cluster due to the uniformity of the magnetic field ( $\nabla B = 0$ ); (iv) the magnetic interactions among clusters are neglected due to the low volume fraction of rods ( $\phi \approx 2 \times 10^{-5}$ ) and the thermal fluctuation of the particle is neglected due to the dominance of the magnetic energy during the structural transition ( $mB/\kappa_B T \geq 500$ , where  $\kappa_B$  is Boltzmann's constant and  $T$  is the room temperature); (v) each cluster consists of  $2N+1$  FMRs, so that we only need to analyze the dynamics of FMRs in one half of the cluster due to the symmetry of the zig-zag chain (a similar derivation for  $2N$  FMRs has also been developed in the ESI,<sup>†</sup> S3).

Since the magnetic moment  $\vec{m}$  of two neighboring rods has different orientations, we shall consider the rods in pairs, *i.e.*, the  $p^{\text{th}}$  rod and the  $(p+1)^{\text{th}}$  rod as shown in Fig. 3b. At the center of the  $p^{\text{th}}$  ( $(p+1)^{\text{th}}$ ) rod, there are hydrodynamic force components  $\vec{F}_{D\perp}^p$  ( $\vec{F}_{D\perp}^{p+1}$ ) and  $\vec{F}_{D\parallel}^p$  ( $\vec{F}_{D\parallel}^{p+1}$ ), which are perpendicular and parallel to the principle axis of the cluster. Here  $\vec{F}_{D\parallel}^p = -\eta \varepsilon_{\parallel} \vec{U}_{\parallel}^p$  and  $\vec{F}_{D\perp}^p = -\eta \varepsilon_{\perp} \vec{U}_{\perp}^p$ , where  $\eta$  is the viscosity of the carrier liquid,  $\varepsilon_{\parallel}$  and  $\varepsilon_{\perp}$  are the hydrodynamic drag coefficients in the direction of  $\vec{U}_{\parallel}^p$  and  $\vec{U}_{\perp}^p$ , and  $\vec{U}_{\parallel}^p$  and  $\vec{U}_{\perp}^p$  are parallel and perpendicular velocities with respect to the chain axis,

respectively,  $\vec{U}_{\parallel}^p = -p\theta \sin \theta \hat{x}$  and  $\vec{U}_{\perp}^p = -p\theta \cos \theta \hat{y}$ . Based on a magnetic charge model,<sup>32</sup> two magnetic forces  $\vec{F}_m^{p+}$  and  $\vec{F}_m^{p-}$  (note that  $F_m^{p+} = F_m^{p-} = F_m$ ) at the + and - ends are presented due to the magnetic polar attraction of the adjacent ends. There are also a normal force  $\vec{F}_n^{p+}$  (or  $\vec{F}_n^{p-}$ ) and a frictional force  $\vec{F}_f^{p+}$  (or  $\vec{F}_f^{p-}$ ) exerted at the interfaces of the + (or -) end due to the contacting interaction and the relative motional tendency between the neighboring rods. Under hydrodynamic equilibrium for a low Reynold number fluid, we have,

$$\vec{F}_n^{p+} + \vec{F}_n^{p-} + \vec{F}_{D\parallel}^p = 0, \quad (1)$$

$$\vec{F}_f^{p+} + \vec{F}_f^{p-} + \vec{F}_{D\perp}^p = 0, \quad (2)$$

$$\vec{I}_m^p + \vec{I}_f^p = 0, \quad (3)$$

where  $\vec{I}_m^p$  is the magnetic driven torque  $\vec{I}_m^p = \vec{m} \times \vec{B} = mB \sin(\varphi + \theta) \hat{z}$ , and  $\vec{I}_f^p$  is the resistant torque,  $\vec{I}_f^p = -\left\{ (F_f^{p-} + F_f^{p+}) \frac{l}{2} \cos \theta + [(F_n^{p-} - F_m^{p-}) + (F_n^{p+} - F_m^{p+})] \frac{l}{2} \sin \theta \right\} \hat{z}$ . Similarly equations can be derived for the  $(p+1)^{\text{th}}$  rod, but with different expressions for  $\vec{I}_m^{p+1} = mB \sin(\varphi - \theta) \hat{z}$  and  $\vec{I}_f^{p+1} = -\left\{ (F_f^{(p+1)-} + F_f^{(p+1)+}) \frac{l}{2} \cos \theta - [(F_n^{(p+1)-} - F_m^{(p+1)-}) + (F_n^{(p+1)+} - F_m^{(p+1)+})] \frac{l}{2} \sin \theta \right\} \hat{z}$ . Furthermore, for the  $p^{\text{th}}$  and

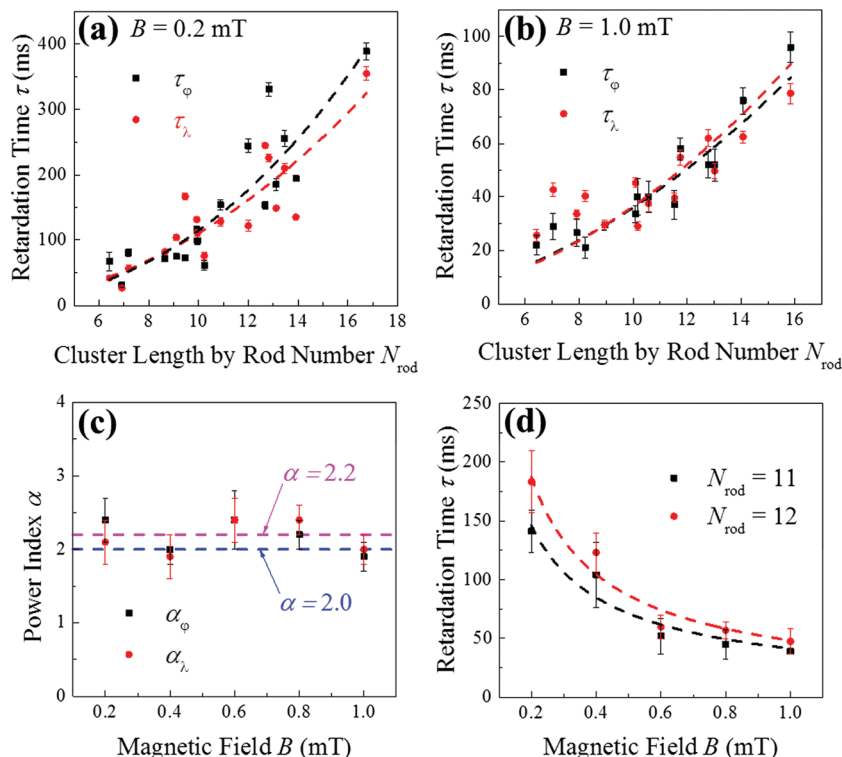


**Fig. 4** The plots of retardation time  $\tau_\lambda$  (red circles) and  $\tau_\phi$  (black squares) versus chain length  $N_{\text{rod}}$  at (a)  $B = 0.2$  mT and (b)  $B = 1.0$  mT. The dashed curves are the fitting by a power law. (c) The plot of exponents  $\alpha_\lambda$  (red circles) and  $\alpha_\phi$  (black squares) for  $B = 0.2, 0.4, 0.6, 0.8,$  and  $1.0$  mT. The average  $\alpha = 2.2$  (pink dashed line) is close to the theoretical prediction  $\alpha = 2$  (blue dashed line). (d) The plots of the average retardation time  $\tau$  versus  $B$  for  $N_{\text{rod}} = 11$  (black squares) and  $12$  (red circles). The dashed curves are the fittings via a power law.

$(p + 1)^{\text{th}}$  rod pair, one has  $\vec{I}_m^p + \vec{I}_m^{p+1} = -(\vec{I}_r^p + \vec{I}_r^{p+1})$  and  $\vec{I}_m^p - \vec{I}_m^{p+1} = -(\vec{I}_r^p - \vec{I}_r^{p+1})$ . By considering the fact that  $F_f^{p+} = F_f^{(p+1)-}$ ,  $F_n^{p+} = F_n^{(p+1)-}$ , and  $F_m^{p+} = F_m^{(p+1)-}$ , we have

$$2mB \sin \varphi \cos \theta = \left( F_f^{p-} + 2F_f^{(p+1)-} + F_f^{(p+1)+} \right) \frac{l}{2} \cos \theta - \left( F_n^{(p+1)+} - F_n^{p-} \right) \frac{l}{2} \sin \theta, \quad (4)$$

$$2mB \cos \varphi \sin \theta = \left[ \left( F_n^{(p+1)+} - F_m^{(p+1)+} \right) + 2 \left( F_n^{(p+1)-} - F_m^{(p+1)-} \right) + \left( F_n^{p-} - F_m^{p-} \right) \right] \frac{l}{2} \sin \theta - \left( F_f^{(p+1)+} - F_f^{p-} \right) \frac{l}{2} \cos \theta. \quad (5)$$

In addition, by summarizing eqn (1) and (2) from the  $(p + 1)^{\text{th}}$  rod to the  $N^{\text{th}}$  rod, respectively, and considering the force equilibrium at the  $N^{\text{th}}$  rod as shown in Fig. 3b, we have  $-\vec{F}_f^{(p+1)-} = \sum_{k=p+1}^N \vec{F}_{D_\perp}^k$  and  $-\vec{F}_n^{(p+1)-} + \vec{F}_m^{(p+1)-} = \sum_{k=p+1}^N \vec{F}_{D_\parallel}^k$ . Therefore, eqn (4) and (5) becomes

$$2mB \sin \varphi \cos \theta = \left( \sum_{k=p+2}^N F_{D_\perp}^k + 2 \sum_{k=p+1}^N F_{D_\perp}^k + \sum_{k=p}^N F_{D_\perp}^k \right) \frac{l}{2} \cos \theta - \left( F_n^{(p+1)+} - F_n^{p-} \right) \frac{l}{2} \sin \theta, \quad (6)$$

$$2mB \cos \varphi \sin \theta = \left( \sum_{k=p}^N F_{D_\parallel}^k + 2 \sum_{k=p+1}^N F_{D_\parallel}^k + \sum_{k=p+2}^N F_{D_\parallel}^k \right) \frac{l}{2} \sin \theta - \left( F_f^{(p+1)+} - F_f^{p-} \right) \frac{l}{2} \cos \theta. \quad (7)$$

Then, eventually by simply summarizing eqn (6) and (7) over all the rod pairs throughout the cluster, all the  $F_n^{(p+1)+}$ ,  $F_n^{p-}$ ,  $F_f^{(p+1)+}$ , and  $F_f^{p-}$  terms are vanished, and the expressions can be further simplified as (see details in the ESI,† S3)

$$\begin{cases} \dot{\theta} = - \left( \frac{3mB}{\varepsilon_\parallel \eta l^2 N^2} \right) \frac{\cos \varphi}{\sin \theta} \\ \dot{\varphi} = - \left( \frac{3mB}{\varepsilon_\perp \eta l^2 N^2} \right) \frac{\sin \varphi}{\cos \theta} \end{cases}. \quad (8)$$

When Stokes flow passes a circular cylinder of small aspect ratio ( $\gamma \leq 10$ ), like the rod in our experiment, the ratio of the hydrodynamic drag coefficients in its long axial direction and in its short axial direction is about 1,<sup>62,63</sup> i.e.,  $\varepsilon_\parallel = \varepsilon_\perp = \varepsilon$ . According to the geometrical relations in Fig. 3b, the normalized length of the chain is approximately estimated to be  $\lambda \approx \cos \theta$ . Therefore, eqn (8) is furtherly simplified as

$$\begin{cases} \dot{\lambda} = \frac{\cos \varphi}{\tau} \\ \dot{\varphi} = - \frac{\sin \varphi}{\tau \lambda} \end{cases}, \quad (9)$$

where  $\tau = \frac{\epsilon\eta l^2 N^2}{3mB}$ . Clearly, the extending and the rotating motions of the rod cluster are coupled together and both of their transient speeds depend on the same parameter  $\tau$ . Eqn (9) can be solved analytically (see details in the ESI,† S4)

$$\begin{cases} \lambda(t) = \sqrt{\left[\left(\frac{t}{\tau}\right) + c_1\right]^2 + c_2}, & \lambda(t) \leq 1 \\ \varphi(t) = \cot^{-1}\left[c_3\left(\frac{t}{\tau}\right) + c_4\right] \end{cases}, \quad (10)$$

where  $c_1 = \lambda_0 \cos \varphi_0$ ,  $c_2 = \lambda_0^2 \sin^2 \varphi_0$ ,  $c_3 = \lambda_0^{-1} \csc \varphi_0$  and  $c_4 = \cot \varphi_0$ , and  $\lambda_0$  and  $\varphi_0$  are the initial values for the cluster. The parameter  $\tau$  has an apparent physical meaning, which describes the competition between the hydrodynamic drag torque and the magnetic torque on a FMRC. It decides the speed of FMRC structural transition by a  $B$ -field and is more complicated than the classic Brownian relaxation time constant of a single magnetic particle.<sup>64,65</sup> The larger  $\tau$  suggests the longer elapsed time for the coupled motion of the cluster. When  $t \ll \tau$ ,  $\lambda(t)$  increases slowly from  $\lambda_0$  and  $\varphi(t)$  decreases rapidly from  $\varphi_0$ . When  $t \gg \tau$ ,  $\lambda(t)$  increases linearly with respect to  $t$  until it reaches 1 and  $\varphi(t)$  slowly approaches 0. Eqn (10) is used to fit the data in Fig. 2b, and both the blue and pink dashed curves represent the best fittings for  $\lambda(t)$  and  $\varphi(t)$ , respectively. The retardation time  $\tau_\lambda$  extracted from the  $\lambda(t)$  fitting is  $30 \pm 2$  ms, and the retardation time  $\tau_\varphi$  extracted from the  $\varphi(t)$  fitting is  $29 \pm 2$  ms, i.e.,  $\tau_\lambda \approx \tau_\varphi$ . Thus the theoretical prediction agrees with experimental data very well.

According to our model, the retardation time  $\tau$  is proportional to  $N^2$  and inversely proportional to  $B$ . Fig. 4a and b plot the  $\tau_\lambda$  (red circles) and  $\tau_\varphi$  (black squares) extracted from different magnetic clusters with different lengths at  $B = 0.2$  mT and 1.0 mT, respectively. Both figures show that  $\tau_\lambda$  and  $\tau_\varphi$  increases monotonically with  $N_{\text{rod}} = L_s/l$ . A power law relationship,  $\tau(N) \sim N^\alpha$ , is used to fit these data. For  $B = 0.2$  mT, one obtains  $\alpha_\lambda = 2.1 \pm 0.3$  (red dashed curve) and  $\alpha_\varphi = 2.4 \pm 0.3$  (black dashed curve); for  $B = 1.0$  mT,  $\alpha_\lambda = 2.0 \pm 0.2$  (red dashed curve) and  $\alpha_\varphi = 1.9 \pm 0.2$  (black dashed curve). Clearly the exponent  $\alpha$  fluctuates around 2.0. In fact, experimentally we extract  $\alpha_\lambda$  and  $\alpha_\varphi$  for  $B = 0.2, 0.4, 0.6, 0.8$  and 1.0 mT, and they are plotted against  $B$  in Fig. 4c. Both  $\alpha_\lambda$  (red circles) and  $\alpha_\varphi$  (black squares) remain constant and the statistical average of all exponent values (including  $\alpha_\lambda$  and  $\alpha_\varphi$ ) is  $\alpha = 2.2 \pm 0.2$  (pink dashed line), which agrees well with the theoretical value,  $\alpha = 2$  (blue dashed line). The relation of  $\tau$  versus  $B$  is also plotted in Fig. 4d. Here we select two groups of clusters with  $N_{\text{rod}} = 11 \pm 0.5$  and  $N_{\text{rod}} = 12 \pm 0.5$ , and  $\tau$  is the average value of the retardation time constants from both  $\tau_\lambda$  and  $\tau_\varphi$ . The  $\tau$  decreases monotonically with  $B$ . By fitting the two data sets with a power law,  $\tau(B) \sim B^\beta$ , we obtain that  $\beta = -0.8 \pm 0.1$ , which is quite close to the theoretical expectation of  $\beta = -1$ . Thus, the model based on the zig-zag chain extension and rotation describes the dynamic extension of the magnetic cluster of FMRCs very well.

## Conclusions

In summary, we have studied in detail the dynamic process of FMRCs under an external magnetic field, and developed a theoretical model based on a zig-zag chain to explain the extending-rotating coupled motion of FMRCs. The origins of this coupled motion come from the field-driven alignment of both FMRs and FMRCs, accompanied by the rearrangement of FMRCs from the side-by-side raft-like structure to the end-to-end chain-like structure. The retardation time constant  $\tau$  derived from the dynamic data of FMRCs of different chain lengths is inversely proportional to the  $B$ -field, and is a square function of the chain length  $N$ , which are consistent with the theoretical prediction. It is expected that this model can be adapted for the dynamics of magnetic clusters consisting of other anisotropic magnetic particles as well as the magneto-elastic behavior of other soft matters consisting of FMRCs.

## Acknowledgements

RC and LM acknowledge the support from the National Science Foundation under the Grant No. ECCS-1150042 and EEC-1359095. LZ, WH, and YZ were funded by National Science Foundation under Contract No. ECCS-1303134. The authors would like to thank Mr Layne Hyer Bradley for proofreading the manuscript.

## References

- 1 A. K. Wanekaya, W. Chen, N. V. Myung and A. Mulchandani, Nanowire-based electrochemical biosensors, *Electroanalysis*, 2006, **18**(6), 533–550.
- 2 D. M. Bruls, T. H. Evers, J. A. H. Kahlman, P. J. W. van Lankvelt, M. Ovsyanko, E. G. M. Pelssers, J. J. H. B. Schleipen, F. K. de Theije, C. A. Verschuren, T. van der Wijk, J. B. A. van Zon, W. U. Dittmer, A. H. J. Immink, J. H. Nieuwenhuis and M. W. J. Prins, Rapid integrated biosensor for multiplexed immunoassays based on actuated magnetic nanoparticles, *Lab Chip*, 2009, **9**(24), 3504–3510.
- 3 P. Martins, A. Larrea, R. Goncalves, G. Botelho, E. V. Ramana, S. K. Mendiratta, V. Sebastian and S. Lanceros-Mendez, Novel Anisotropic Magnetolectric Effect on delta-FeO(OH)/P(VDF-TrFE) Multiferroic Composites, *ACS Appl. Mater. Interfaces*, 2015, **7**(21), 11224–11229.
- 4 A. Rida and M. A. M. Gijs, Manipulation of self-assembled structures of magnetic beads for microfluidic mixing and assaying, *Anal. Chem.*, 2004, **76**(21), 6239–6246.
- 5 Y. Gao, M. A. Hulsen, T. G. Kang and J. M. J. den Toonder, Numerical and experimental study of a rotating magnetic particle chain in a viscous fluid, *Phys. Rev. E: Stat., Nonlinear, Soft Matter Phys.*, 2012, **86**(4), 041503.
- 6 Y. Gao, A. van Reenen, M. A. Hulsen, A. M. de Jong, M. W. J. Prins and J. M. J. den Toonder, Disaggregation of microparticle clusters by induced magnetic dipole–dipole repulsion near a surface, *Lab Chip*, 2013, **13**(7), 1394–1401.

- 7 A. van Reenen, A. M. de Jong, J. M. J. den Toonder and J. W. M. Prins, Integrated lab-on-chip biosensing systems based on magnetic particle actuation – a comprehensive review, *Lab Chip*, 2014, **14**(12), 1966–1986.
- 8 J. Philip, T. Jaykumar, P. Kalyanasundaram and B. Rai, A tunable optical filter, *Meas. Sci. Technol.*, 2003, **14**(8), 1289–1294.
- 9 S. L. Pu, X. F. Chen, L. J. Chen, W. J. Liao, Y. P. Chen and Y. X. Xia, Tunable magnetic fluid grating by applying a magnetic field, *Appl. Phys. Lett.*, 2005, **87**(2), 021901.
- 10 T. Liu, X. Chen, Z. Di, J. Zhang, X. Li and J. Chen, Tunable magneto-optical wavelength filter of long-period fiber grating with magnetic fluids, *Appl. Phys. Lett.*, 2007, **91**(12), 121116.
- 11 J. Philip, P. D. Shima and B. Raj, Nanofluid with tunable thermal properties, *Appl. Phys. Lett.*, 2008, **92**(4), 043108.
- 12 S. A. Angayarkanni and J. Philip, Review on thermal properties of nanofluids: recent developments, *Adv. Colloid Interface Sci.*, 2015, **225**, 146–176.
- 13 P. Y. Keng, I. Shim, B. D. Korth, J. F. Douglas and J. Pyun, Synthesis and self-assembly of polymer-coated ferromagnetic nanoparticles, *ACS Nano*, 2007, **1**(4), 279–292.
- 14 A. Tokarev, Y. Gu, A. Zakharchenko, O. Trotsenko, I. Luzinov, K. G. Kornev and S. Minko, Reconfigurable Anisotropic Coatings via Magnetic Field-Directed Assembly and Translocation of Locking Magnetic Chains, *Adv. Funct. Mater.*, 2014, **24**(30), 4738–4745.
- 15 M. G. Zahedi, D. Lorenzo, R. Brescia, R. Ruffilli, I. Liakos, T. Pellegrino, A. Athanassiou and D. Fragouli, Magnetic-Field-Induced Formation of Superparamagnetic Microwires in Suspension, *J. Phys. Chem. C*, 2014, **118**(48), 28220–28226.
- 16 J. Kim, S. E. Chung, S. E. Choi, H. Lee, J. Kim and S. Kwon, Programming magnetic anisotropy in polymeric microactuators, *Nat. Mater.*, 2011, **10**(10), 747–752.
- 17 F. Xu, C. A. M. Wu, V. Rengarajan, T. D. Finley, H. O. Keles, Y. R. Sung, B. Q. Li, U. A. Gurkan and U. Demirci, Three-Dimensional Magnetic Assembly of Microscale Hydrogels, *Adv. Mater.*, 2011, **23**(37), 4254–4260.
- 18 S. Tasoglu, C. H. Yu, H. I. Gungordu, S. Guven, T. Vural and U. Demirci, Guided and magnetic self-assembly of tunable magnetoceptive gels, *Nat. Commun.*, 2014, **5**, 4702.
- 19 G. Helgesen, A. T. Skjeltorp, P. M. Mors, R. Botet and R. Jullien, Aggregation of Magnetic Microspheres – Experiments and Simulations, *Phys. Rev. Lett.*, 1988, **61**(15), 1736–1739.
- 20 M. Fermigier and A. P. Gast, Structure Evolution in a Paramagnetic Latex Suspension, *J. Colloid Interface Sci.*, 1992, **154**(2), 522–539.
- 21 J. H. E. Promislow, A. P. Gast and M. Fermigier, Aggregation Kinetics of Paramagnetic Colloidal Particles, *J. Chem. Phys.*, 1995, **102**(13), 5492–5498.
- 22 M. C. Miguel and R. Pastor-Satorras, Kinetic growth of field-oriented chains in dipolar colloidal solutions, *Phys. Rev. E: Stat. Phys., Plasmas, Fluids, Relat. Interdiscip. Top.*, 1999, **59**(1), 826–834.
- 23 J. Garcia-Otero, M. Porto, J. Rivas and A. Bunde, Influence of dipolar interaction on magnetic properties of ultrafine ferromagnetic particles, *Phys. Rev. Lett.*, 2000, **84**(1), 167–170.
- 24 S. Melle, M. A. Rubio and G. G. Fuller, Time scaling regimes in aggregation of magnetic dipolar particles: scattering dichroism results, *Phys. Rev. Lett.*, 2001, **87**(11), 115501.
- 25 C. Dominik and H. Nubold, Magnetic aggregation: dynamics and numerical Modeling, *Icarus*, 2002, **157**(1), 173–186.
- 26 E. Climent, M. R. Maxey and G. E. Karniadakis, Dynamics of self-assembled chaining in magnetorheological fluids, *Langmuir*, 2004, **20**(2), 507–513.
- 27 F. Martinez-Pedrero, M. Tirado-Miranda, A. Schmitt and J. Callejas-Fernandez, Formation of magnetic filaments: a kinetic study, *Phys. Rev. E: Stat., Nonlinear, Soft Matter Phys.*, 2007, **76**(1), 011405.
- 28 J. de Vicente, J. P. Segovia-Gutierrez, E. Andablo-Reyes, F. Vereda and R. Hidalgo-Alvarez, Dynamic rheology of sphere- and rod-based magnetorheological fluids, *J. Chem. Phys.*, 2009, **131**(19), 194902.
- 29 P. Dominguez-Garcia and M. A. Rubio, Three-dimensional morphology of field-induced chain-like aggregates of superparamagnetic microparticles, *Colloids Surf., A*, 2010, **358**(1–3), 21–27.
- 30 P. Dominguez-Garcia, J. M. Pastor and M. A. Rubio, Aggregation and disaggregation dynamics of sedimented and charged superparamagnetic micro-particles in water suspension, *Eur. Phys. J. E: Soft Matter Biol. Phys.*, 2011, **34**(4), 36.
- 31 Z. J. Tan, X. W. Zou, W. B. Zhang and Z. Z. Jin, Structure transition in cluster-cluster aggregation under external fields, *Phys. Rev. E: Stat. Phys., Plasmas, Fluids, Relat. Interdiscip. Top.*, 2000, **62**(1), 734–737.
- 32 M. Aoshima and A. Satoh, Two-dimensional Monte Carlo simulations of a colloidal dispersion composed of rod-like ferromagnetic particles in an applied magnetic field, *Model. Numer. Simul. Mater. Sci.*, 2008, **16**(1), 015004.
- 33 H. Morimoto and T. Maekawa, Cluster structures and cluster-cluster aggregations in a two-dimensional ferromagnetic colloidal system, *J. Phys. A: Math. Gen.*, 2000, **33**(2), 247–258.
- 34 S. K. Smoukov, S. Gangwal, M. Marquez and O. D. Velev, Reconfigurable responsive structures assembled from magnetic Janus particles, *Soft Matter*, 2009, **5**(6), 1285–1292.
- 35 L. Baraban, D. Makarov, M. Albrecht, N. Rivier, P. Leiderer and A. Erbe, Frustration-induced magic number clusters of colloidal magnetic particles, *Phys. Rev. E: Stat., Nonlinear, Soft Matter Phys.*, 2008, **77**(3), 031407.
- 36 S. Kantorovich, R. Weeber, J. J. Cerda and C. Holm, Ferrofluids with shifted dipoles: ground state structures, *Soft Matter*, 2011, **7**(11), 5217–5227.
- 37 E. V. Novak, E. S. Pyanzina and S. S. Kantorovich, Behaviour of magnetic Janus-like colloids, *J. Phys.: Condens. Matter*, 2015, **27**(23), 234102.
- 38 M. R. Dudek and K. W. Wojciechowski, Magnetic films of negative Poisson's ratio in rotating magnetic fields, *J. Non-Cryst. Solids*, 2008, **354**(35–39), 4304–4308.
- 39 J. N. Grima, R. Caruana-Gauci, M. R. Dudek, K. W. Wojciechowski and R. Gatt, Smart metamaterials with tunable auxetic and other properties, *Smart Mater. Struct.*, 2013, **22**(8), 084016.

- 40 S. Chikazumi, C. D. Graham and S. Chikazumi, *Physics of ferromagnetism*, Clarendon Press, Oxford, 2nd edn, 1997, vol. 7, p. 655.
- 41 R. Skomski, *Nanomagnetics*, *J. Phys.: Condens. Matter*, 2003, **15**(20), R841–R896.
- 42 A. Tokarev, B. Rubin, M. Bedford and K. G. Kornev, *Magnetic Nanorods for Optofluidic Applications*, *AIP Conf. Proc.*, 2010, **1311**, 204–209.
- 43 M. K. Gupta, D. D. Kulkarni, R. Geryak, S. Naik and V. V. Tsukruk, *A Robust and Facile Approach To Assembling Mobile and Highly-Open Unfrustrated Triangular Lattices from Ferromagnetic Nanorods*, *Nano Lett.*, 2013, **13**(1), 36–42.
- 44 J. Townsend, R. Burtovyy, Y. Galabura and I. Luzinov, *Flexible Chains of Ferromagnetic Nanoparticles*, *ACS Nano*, 2014, **8**(7), 6970–6978.
- 45 M. Aoshima and A. Satoh, *Two-dimensional Monte Carlo simulations of a colloidal dispersion composed of rod-like ferromagnetic particles in the absence of an applied magnetic field*, *J. Colloid Interface Sci.*, 2006, **293**(1), 77–87.
- 46 C. T. Lo and W. T. Lin, *Effect of Rod Length on the Morphology of Block Copolymer/Magnetic Nanorod Composites*, *J. Phys. Chem. B*, 2013, **117**(17), 5261–5270.
- 47 C. T. Lo and K. H. Tsui, *The dispersion of magnetic nanorods in poly(2-vinylpyridine)*, *Polym. Int.*, 2013, **62**(11), 1652–1658.
- 48 F. X. Ma, H. B. Wu, C. Y. Xu, L. Zhen and X. W. Lou, *Self-organized sheaf-like Fe<sub>3</sub>O<sub>4</sub>/C hierarchical microrods with superior lithium storage properties*, *Nanoscale*, 2015, **7**(10), 4411–4414.
- 49 R. F. Butler and S. K. Banerjee, *Theoretical Single-Domain Grain-Size Range in Magnetite and Titanomagnetite*, *J. Geophys. Res.*, 1975, **80**(29), 4049–4058.
- 50 L. Thomas, R. Moriya, C. Rettner and P. S. S. Parkin, *Dynamics of Magnetic Domain Walls Under Their Own Inertia*, *Science*, 2010, **330**(6012), 1810–1813.
- 51 M. Jamali, K. J. Lee and H. Yang, *Metastable magnetic domain wall dynamics*, *New J. Phys.*, 2012, **14**, 033010.
- 52 A. Pivano and V. O. Dolocan, *Chaotic dynamics of magnetic domain walls in nanowires*, *Phys. Rev. B: Condens. Matter Mater. Phys.*, 2016, **93**(14), 144410.
- 53 C. P. Bean, *Hysteresis Loops of Mixtures of Ferromagnetic Micropowders*, *J. Appl. Phys.*, 1955, **26**(11), 1381–1383.
- 54 A. S. Silva, R. Bond, F. Plouraboue and D. Wirtz, *Fluctuation dynamics of a single magnetic chain*, *Phys. Rev. E: Stat. Phys., Plasmas, Fluids, Relat. Interdiscip. Top.*, 1996, **54**(5), 5502–5510.
- 55 D. E. Smith, H. P. Babcock and S. Chu, *Single-polymer dynamics in steady shear flow*, *Science*, 1999, **283**(5408), 1724–1727.
- 56 T. Sakaue and K. Yoshikawa, *Folding/unfolding kinetics on a semiflexible polymer chain*, *J. Chem. Phys.*, 2002, **117**(13), 6323–6330.
- 57 W. A. Linke, M. Ivemeyer, N. Olivieri, B. Kolmerer, J. C. Ruegg and S. Labeit, *Towards a molecular understanding of the elasticity of titin*, *J. Mol. Biol.*, 1996, **261**(1), 62–71.
- 58 M. Rief, M. Gautel, F. Oesterhelt, J. M. Fernandez and H. E. Gaub, *Reversible unfolding of individual titin immunoglobulin domains by AFM*, *Science*, 1997, **276**(5315), 1109–1112.
- 59 L. Tskhovrebova, J. Trinick, J. A. Sleep and R. M. Simmons, *Elasticity and unfolding of single molecules of the giant muscle protein titin*, *Nature*, 1997, **387**(6630), 308–312.
- 60 P. J. Flory, *Statistical mechanics of chain molecules*, Hanser Publishers, Distributed in the U.S.A. by Oxford University Press, Munich, New York, Repr edn, 1989, p. xxv, p. 432.
- 61 J. S. Kim and S. R. G. Chirikjian, *A unified approach to conformational statistics of classical polymer and polypeptide models*, *Polymer*, 2005, **46**(25), 11904–11917.
- 62 G. Batchelo, *Slender-Body Theory for Particles of Arbitrary Cross-Section in Stokes Flow*, *J. Fluid Mech.*, 1970, **44**(Nov26), 419–440.
- 63 R. E. Johnson, *An Improved Slender-Body Theory for Stokes-Flow*, *J. Fluid Mech.*, 1980, **99**(Jul), 411–431.
- 64 A. Tokarev, I. Luzinov, J. R. Owens and K. G. Kornev, *Magnetic Rotational Spectroscopy with Nanorods to Probe Time-Dependent Rheology of Microdroplets*, *Langmuir*, 2012, **28**(26), 10064–10071.
- 65 A. Gunther, P. Bender, A. Tschope and R. Birringer, *Rotational diffusion of magnetic nickel nanorods in colloidal dispersions*, *J. Phys.: Condens. Matter*, 2011, **23**(32), 325103.